

## Perturbational view of inherent structures in water

Frank H. Stillinger and Teresa Head-Gordon  
*AT&T Bell Laboratories, Murray Hill, New Jersey 07974*  
 (Received 14 October 1992)

The existence of accurately measured oxygen pair-correlation functions for liquid water suggests a natural form of linear perturbation theory for that substance. The unperturbed potential involves isotropically interacting molecules, and reproduces the measured oxygen-pair short-range order. Monte Carlo simulations in this theoretical context have been carried out for the unperturbed system and for the fully coupled system in the liquid state at 25°C. Inherent structures (potential-energy minima) have been generated and examined in both of these cases; they demonstrate that the directionality intrinsic to hydrogen bonding plays an important role in structurally stabilizing short-range order at the pair and higher-order correlation levels.

PACS number(s): 61.20.Ne, 61.25.Em

### I. INTRODUCTION

The inherent structure concept for condensed phases [1–3], and its numerical applications [4–6], have generated novel insights into a wide variety of physical and chemical phenomena [7–12]. In particular, it has been valuable to identify and to classify the inherent structures (potential-energy minima) in water [13–16], and to follow their chronological sequence during molecular-dynamics simulation by steepest-descent mapping [17–19].

This paper examines inherent structures in water from a somewhat unconventional standpoint. The water interactions, as explained below, are theoretically embedded in a perturbational format. When the relevant perturbation parameter  $\lambda$  vanishes, we have a simple, but nontrivial, reference model. Increasing  $\lambda$  to the “physical” value unity restores the proper water molecule interactions. It has been our objective to compare and to contrast the inherent structures present in the system at both extremes  $\lambda=0$  and 1 to attain new insights.

Section II defines and explains our perturbation scheme. Section III presents properties of the  $\lambda=0$  reference model, including inherent structures, emerging from Monte Carlo simulation. Section IV does the same for the  $\lambda=1$  “real water” case. Section V draws some important conclusions.

### II. PERTURBATION MODEL

We require that the molecular assembly of water molecules be represented by an interaction potential  $\Phi(\mathbf{x}_1, \dots, \mathbf{x}_N; \lambda)$  that is linear in perturbation coupling constant  $\lambda$ ,

$$\Phi(\mathbf{x}_1, \dots, \mathbf{x}_N; \lambda) = (1 - \lambda)\Phi_0(\mathbf{r}_1, \dots, \mathbf{r}_N) + \lambda\Phi_1(\mathbf{x}_1, \dots, \mathbf{x}_N). \quad (2.1)$$

Here  $\mathbf{x}_i$  comprises position and orientation coordinates for molecule  $i$ , while  $\mathbf{r}_i$  denotes the location of its oxygen nucleus. For present purposes it suffices to suppose that the water molecules are rigid, and that in the liquid state they can be described by classical statistical mechanics.

The criteria applied in selection of the unperturbed interaction  $\Phi_0$  were (i) that it consists of an additive sum of central pair potentials acting between oxygens,

$$\Phi_0(\mathbf{r}_1, \dots, \mathbf{r}_N) = \sum_{\substack{i,j \\ i < j}} v_0(r_{ij}), \quad (2.2)$$

and (ii) that it alone will closely reproduce the measurable oxygen short-range order in the water system at the given temperature  $T$  and density  $\rho$ . This short-range order is encompassed in the oxygen-oxygen pair-correlation function  $g_{OO}(r)$  that is provided by diffraction experiments. With  $\lambda=0$ , so that only  $\Phi_0$  operates between the water molecules, rotations about the oxygen centers are entirely free.

As  $\lambda$  increases from 0 to 1, torques develop between neighboring molecules. In the fully coupled limit  $\lambda=1$  these torques describe formation of linear hydrogen bonds between neighbors. It is generally conceded that interactions in “real” water can adequately be described by a sum of intermolecular pair potentials, i.e.,

$$\Phi_0 + \Phi_1 = \sum_{\substack{i,j \\ i < j}} V^{(2)}(\mathbf{x}_i, \mathbf{x}_j), \quad (2.3)$$

where now of course the orientational degrees of freedom explicitly come into play. The literature contains several approximate forms that could be used for  $V^{(2)}$  [20–23].

We have utilized the hypernetted chain (HNC) approximation [24] to infer  $v_0$  from the experimental  $g_{OO}(r)$ ,

$$v_0(r) \cong k_B T [g_{OO}(r) - 1 - \ln g_{OO}(r) - C(r)]. \quad (2.4)$$

Here  $C(r)$  is the oxygen-oxygen direct-correlation function, defined in terms of  $g_{OO}(r)$  by the Ornstein-Zernike integral equation [25],

$$C(r_{12}) = g_{OO}(r_{12}) - 1 - \rho \int C(r_{13}) [g_{OO}(r_{32}) - 1] d\mathbf{r}_3. \quad (2.5)$$

Figure 1 displays the experimental  $g_{OO}$  determined for liquid water at 25°C by Soper and Phillips [26], using neutron diffraction. Figure 2 shows the resulting effective

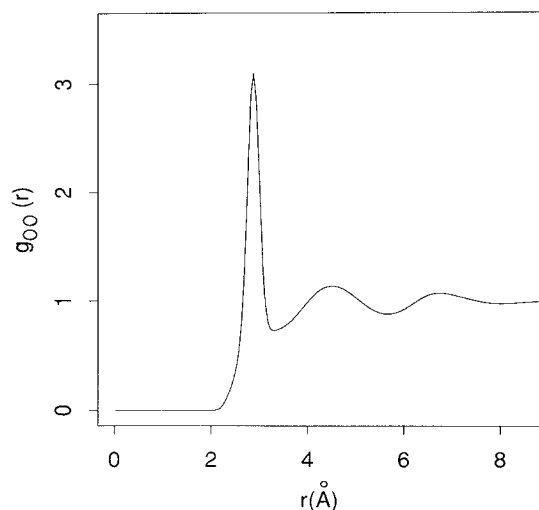


FIG. 1. Experimental oxygen-oxygen pair-correlation function for liquid water at 25°C, from Soper and Phillips (Ref. [26]).

pair potential  $v_0(r)$ . Appendix A provides an accurate analytical fit to  $v_0(r)$  that we have found useful for our Monte Carlo calculations. It is clear from Fig. 2 that  $v_0$  is qualitatively unlike any of the other pair interactions that have been employed previously in liquid state studies, such as the venerable Lennard-Jones interaction.

The obvious next step is to verify the extent to which criterion (ii) above is fulfilled by the calculated  $v_0(r)$ . For this purpose we have carried out a Metropolis Monte Carlo simulation [27] for 216 molecules subject only to interaction  $\Phi_0$ , in a cubic unit cell with periodic boundary conditions. Temperature was fixed at 25°C, and the number density was set at the experimental value ( $0.0334277 \text{ \AA}^{-3}$ ). Pair interactions were truncated at half the cell side length ( $9.313 \text{ \AA}$ ). Following a prolonged equilibration calculation ( $1 \times 10^6$  steps),  $g_{00}$  in

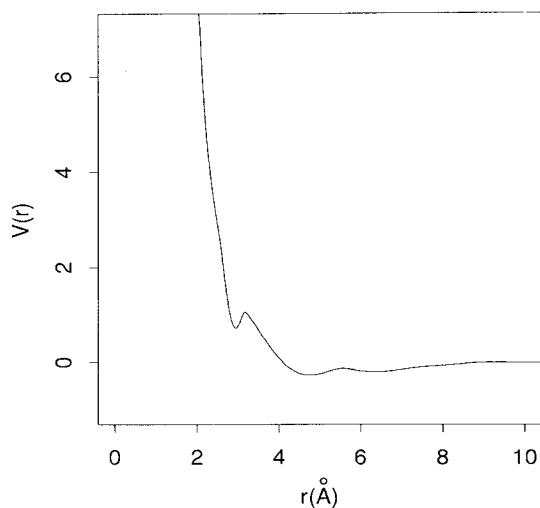


FIG. 2. Effective pair potential  $v_0$  acting between oxygen atoms, for liquid water at 25°C.

this unperturbed model system was evaluated over a  $5 \times 10^5$ -step Monte Carlo run (with approximately 50% configurational-change acceptance rate). Figure 3 shows the result, along with the Soper and Phillips result for comparison. While the extent of agreement is reasonably good, there are clearly some minor discrepancies, and we suspect these are primarily attributable to the error in the HNC approximation, Eq. (2.4), for the present application. In any event the short-range oxygen order in the  $\Phi_0$  unperturbed state is distinctly waterlike, with 4.584 nearest neighbors on average out to a cutoff distance  $r_c = 3.36 \text{ \AA}$  (compared to 4.603 with the same  $r_c$  for the Soper-Phillips experimental  $g_{00}$ ). No doubt some functional fine tuning of  $v_0$  could reduce the discrepancies in Fig. 3, but for present purposes this is unnecessary.

The “real water” pair interaction  $V^{(2)} \equiv v_0 + v_1$  that has been used in our perturbed system calculations is a variant of the “ST2” pair potential [20]. Its details are presented in Appendix B.

The linear perturbational format defined by Eq. (2.1) and the additive forms for  $\Phi_0$ , Eq. (2.2), and for  $\Phi_1$ , Eq. (2.3), are well suited for development of a statistical-mechanical perturbation theory of the liquid state. Its details will be presented in a separate publication [28]. The present project concentrates just on the end points  $\lambda=0$  and 1.

Monte Carlo calculations have also been carried out for the fully coupled case,  $\lambda=1$ , where  $\Phi_0 + \Phi_1$  provides the intermolecular interactions. The same system size, boundary conditions, run length, and temperature applied; the last  $\lambda=0$  configuration supplied the starting point. But, in addition, pair interactions were disregarded beyond distance  $8.5 \text{ \AA}$  between the oxygens, to facilitate the computations. Figure 4 displays the oxygen-oxygen pair-correlation function for this case, along with the Soper-Phillips experimental function. Once again there are minor discrepancies, this time owing primarily

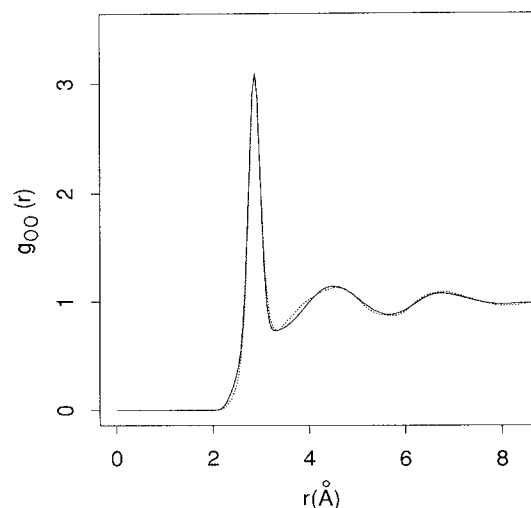


FIG. 3. Comparison of the  $\lambda=0$  oxygen-oxygen pair-correlation function at 25°C obtained by Monte Carlo simulation (dotted curve) with the Soper-Phillips experimental result (solid curve).

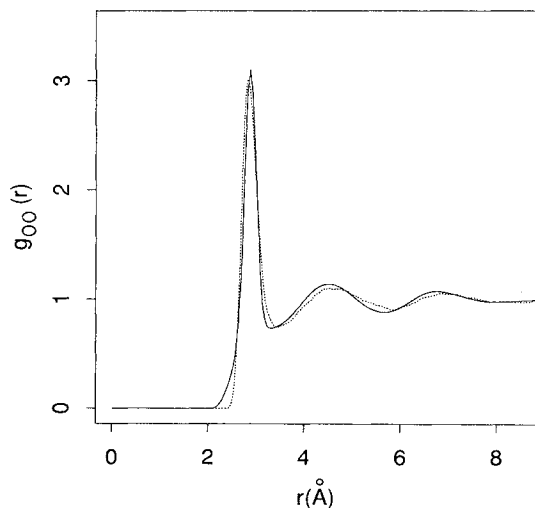


FIG. 4. Comparison of the  $\lambda=1$  oxygen-oxygen pair-correlation function at 25° from simulation (dotted curve) with the Soper-Phillips experimental result (solid curve).

to error in the chosen model potential. Nevertheless, the computed oxygen-pair short-range order is again reasonably faithful to the distinctive characteristics that set water apart from other molecular liquids. Using the same cutoff convention as before ( $r_c = 3.36 \text{ \AA}$ ), the mean number of nearest neighbors found from the  $\lambda=1$  Monte Carlo  $g_{OO}$  is 4.850 (experimental value 4.603).

By construction the rotations of the water molecules are entirely free at  $\lambda=0$ . This implies that the potential-energy minima are manifolds of dimension  $3N+3$  when periodic boundary conditions are present. All structural information is present just in the oxygen atom distribution functions when the system is in this uncoupled state. But any increase in  $\lambda$  above zero, however small, will eliminate the rotational degeneracy and reduce the dimension of the potential-minimum manifolds to 3. As a result, distribution functions involving hydrogen atoms become relevant in specifying structure in the system.

### III. $\lambda=0$ INHERENT STRUCTURES

During the course of the Monte Carlo simulation for the unperturbed reference model, 50 system configurations were stored for later mapping onto their respective inherent structures. These configurations were separated one from the next by  $10^4$  Monte Carlo steps. The subsequent mapping onto potential-energy minima involved direct numerical solution of the steepest-descent equations [1]. Various properties were then evaluated as averages over these 50 inherent structures for the unperturbed reference state. The mean values of the interaction energy per particle before and after mapping to minima are the following:

$$\langle \Phi_0/N \rangle = \begin{cases} -2.285 \text{ kcal/mol} \\ \text{(liquid at 25°C) ,} \\ -3.335 \text{ kcal/mol} \\ \text{(inherent structures) .} \end{cases} \quad (3.1)$$

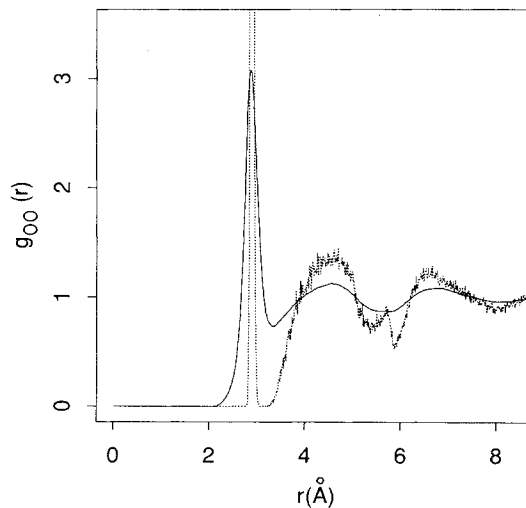


FIG. 5. Inherent-structure pair-correlation function for the  $\lambda=0$  reference state (dotted curve), along with its unmapped simulation precursor (solid curve) in the 25°C liquid.

Figure 5 shows  $g_{OO}$  for the  $\lambda=0$  inherent structures, along with the same quantity prior to mapping to minima. Comparison of the two curves demonstrates the effect of removing intrabasin vibrational deformation. As usual this reduction to potential-energy minima, the inherent structures, markedly amplifies and clarifies the image of short-range order. Indeed, the first-neighbor peak of the inherent-structure  $g_{OO}$  has become separated by an unoccupied gap. Furthermore, the second and third peaks of the premapping  $g_{OO}$  have become substantially more distinct after mapping, and an unsuspected weak peak has arisen between them, centered near 5.7  $\text{\AA}$ .

The narrow first peak in the inherent structure curve of Fig. 5 coincides in distance with a narrow, shallow, but distinctive minimum that is obvious in the plot of the effective central pair potential in Fig. 2. Evidently this positive-energy feature in  $v_0$  traps approximately the correct number of neighbors at 25°C to simulate water-

TABLE I. Distribution of nearest neighbors from the corresponding simulations with  $r_c = 3.36 \text{ \AA}$ .

$n$	$\lambda=0$ , 25°C equilibrium liquid	$\lambda=0$ inherent structures	$\lambda=1$ , 25°C equilibrium liquid	$\lambda=1$ inherent structures
0	0.000	0.000	0.000	0.000
1	0.003	0.001	0.000	0.000
2	0.030	0.017	0.006	0.002
3	0.130	0.109	0.061	0.054
4	0.292	0.298	0.319	0.441
5	0.327	0.362	0.342	0.315
6	0.173	0.179	0.189	0.143
7	0.041	0.032	0.064	0.040
8	0.005	0.002	0.009	0.004
9	0.000	0.000	0.001	0.000
10	0.000	0.000	0.000	0.000
$\langle n \rangle$	4.584	4.687	4.850	4.670

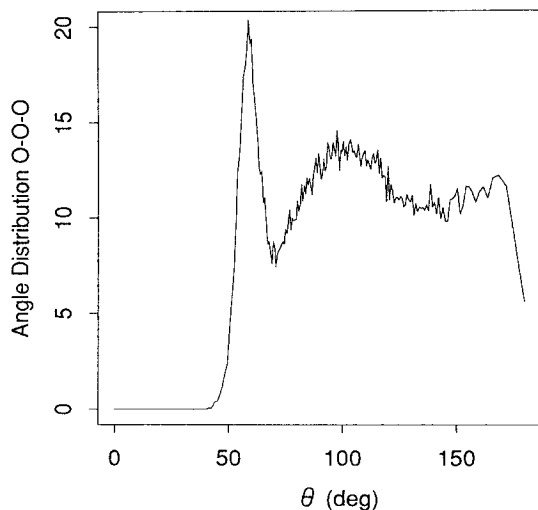


FIG. 6. Distribution of angles to nearest neighbors in the  $\lambda=0$  liquid at 25°C.

like short-range order. The previously used cutoff  $r_c = 3.36 \text{ \AA}$  falls just at the far side of the vacated gap in Fig. 5, so the continued use of this distance criterion is still valid to compute the mean number of nearest neighbors in the inherent structures; we find 4.656 for this quantity.

The first two columns of Table I contain the distributions of coordination numbers, using the same cutoff criterion, for the  $\lambda=0$  liquid before and after reduction to inherent structures. Evidently the removal of vibrational distortion narrows the distribution somewhat, and shifts the mean slightly to a higher value.

Figures 6 and 7 present the distributions of angles between neighbors subtended at a central particle, respectively prior to, and after, mapping to potential minima. Once again we observe substantial enhancement of the lo-

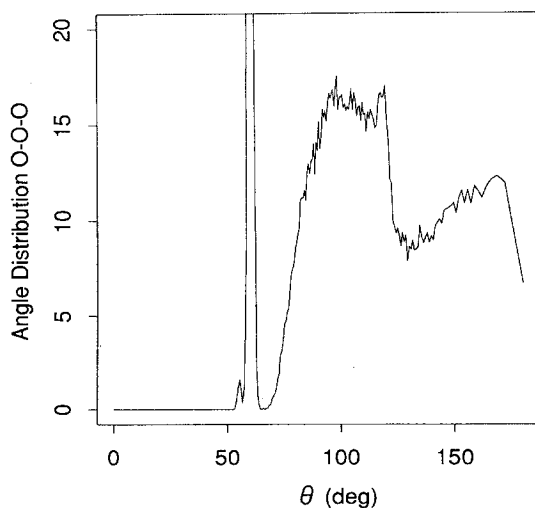


FIG. 7. Distribution of angles to nearest neighbors for the  $\lambda=0$  inherent structures.

cal order. Broad features are present in both distributions around the tetrahedral angle  $\theta_t = \cos^{-1}(-\frac{1}{3}) \approx 109.5^\circ$ . However, the most prominent characteristic is a peak near  $60^\circ$ , already narrow in Fig. 6 and much more so in Fig. 7. Doubtless these correspond to essentially equilateral triangles of particles mutually caught in the metastable minima of the interactions  $v_0(r_{ij})$ . Note also that a substantial number of neighbor pairs exhibit large angles, i.e., are almost in a linear arrangement. These last may well account for the small but distinctive feature at  $5.7 \text{ \AA}$  in the inherent structure  $g_{OO}$ , Fig. 5.

#### IV. $\lambda=1$ INHERENT STRUCTURES

With the unperturbed model results as background, we next examine the inherent structures for the fully coupled water system. First we note the mean values of the interaction energy per water molecule, corresponding to those shown earlier in Eq. (3.1),

$$\langle (\Phi_0 + \Phi_1) / N \rangle = \begin{cases} -9.378 \text{ kcal/mol} \\ \text{(liquid at 25°C)}, \\ -11.616 \text{ kcal/mol} \\ \text{(inherent structures)}. \end{cases} \quad (4.1)$$

The first of these can be compared with the experimental value of the binding energy per molecule in the 25°C liquid,  $-9.77 \text{ kcal/mol}$  [29]. The second is an average over 50 individual inherent structures, computed from starting configurations sequentially separated by  $10^4$  steps in the Monte Carlo run; as in the  $\lambda=0$  case these were obtained by integrating steepest-descent equations numerically.

Figure 8 displays the  $g_{OO}(r)$  for the  $\lambda=1$  inherent structures, along with the premapping function for the  $\lambda=1$ , 25°C liquid. The former should also be compared to the analogous  $\lambda=0$  result in Fig. 5. While a significant

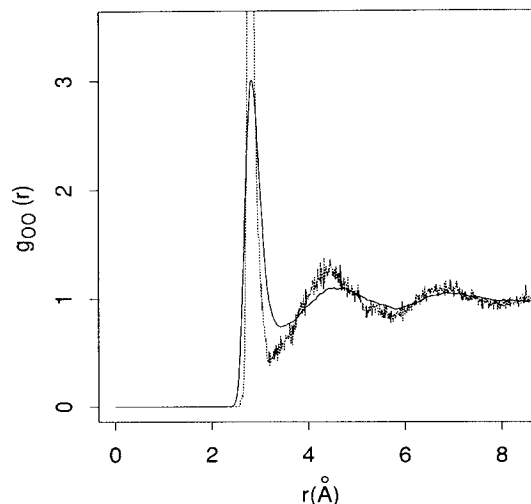


FIG. 8. Inherent-structure pair-correlation function for the  $\lambda=1$  system (dashed curve), and its unmapped simulation precursor (solid curve) in the 25°C liquid.

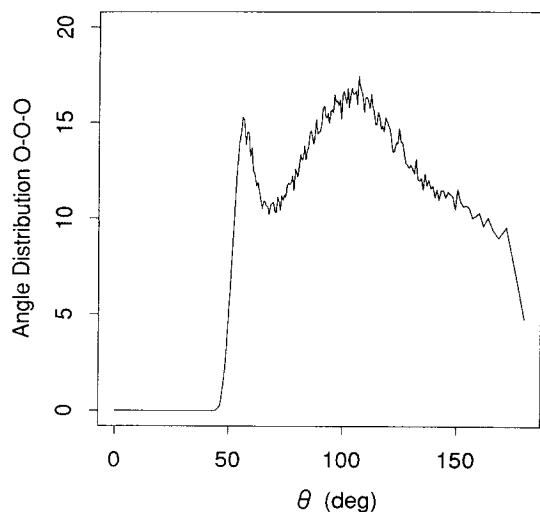


FIG. 9. Distribution of angles to nearest neighbors in the fully coupled ( $\lambda=1$ ) simulation liquid at 25°C.

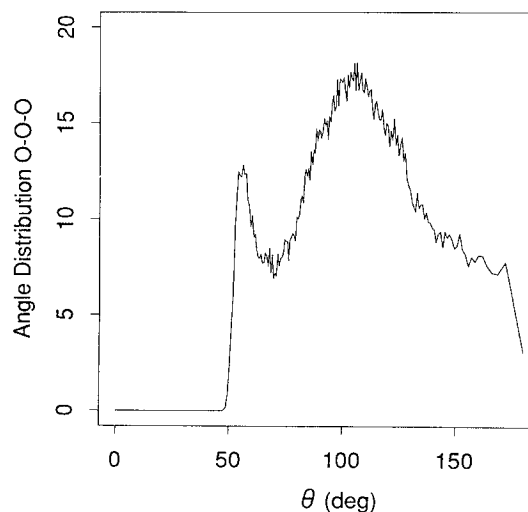


FIG. 10. Distribution of angles to nearest neighbors for the  $\lambda=1$  inherent structures.

sharpening of the image of short-range order has occurred, its extent is substantially less than was found at  $\lambda=0$ . The first peak has narrowed less in the present case, and has not been separated by a vacant gap from the remainder of the pair distance distribution. Furthermore, the second and third  $g_{OO}(r)$  peaks (particularly the latter) have been relatively resistant to change under mapping to potential-energy minima. It must be kept in mind that these clear differences between the  $\lambda=0$  and 1 cases have emerged in spite of the fact that both started with very similar premapping short-range oxygen-atom orders at the pair level.

The latter two columns in Table I show the premapping and post-mapping distributions of coordination numbers for  $\lambda=1$ . Once again we observe that removal of vibrational distortion narrows the distribution, but now shifts the mean a bit to a lower value.

Figure 9 contains the angle distribution for pairs of neighbor oxygens in the coordination shell of any given oxygen, for the  $\lambda=1$ , 25°C liquid. Figure 10 presents the corresponding distribution after mapping to inherent structures. Probably the most illuminating feature that these plots convey is the presence once again of compact, nearly equilateral, triangles, though they are less frequently encountered than before. Clearly these are not elements of a random tetrahedral network, but are associated with local breakdown of tetrahedrality. Nevertheless, broad peaks centered near the tetrahedral angle  $\theta$ , are also obvious in Figs. 9 and 10, so roughly linear hydrogen bonds are present in profusion.

It was pointed out that comparison of the inherent structure  $g_{OO}$ 's in Figs. 5 and 8 showed the fully coupled liquid to be more resistant to short-range-order sharpening than was the uncoupled ( $\lambda=0$ ) liquid. A similar message emerges from the angle distributions. The changes effected by mapping at  $\lambda=1$ , passing from Fig. 9 to Fig. 10, is relatively less than the corresponding changes illustrated by Figs. 6 and 7 for  $\lambda=0$ . Evidently directed hydrogen bonds lock in structure so vibrations are less

effective in delocalizing oxygens.

The intermolecular pair cross-correlation function  $g_{OH}(r)$  for the  $\lambda=1$ , 25°C liquid appears in Fig. 11. The Soper-Phillips experimental function is included for comparison. It is fair to say that overall the agreement is good. The first peak of  $g_{OH}(r)$  is clearly to be associated with the presence of nearly linear hydrogen bonds. Using a cutoff distance criterion  $r_c(\text{OH})=2.35$  Å, the mean number of H's surrounding any O is found to be 1.86 and 1.66 for the simulational and experimental liquids, respectively. This number is 2 in ice, of course.

Figure 12 exhibits the intermolecular pair cross-correlation function  $g_{OH}(r)$  for the inherent structures. The premapping function is included for comparison. Substantial sharpening of the first and second peaks has

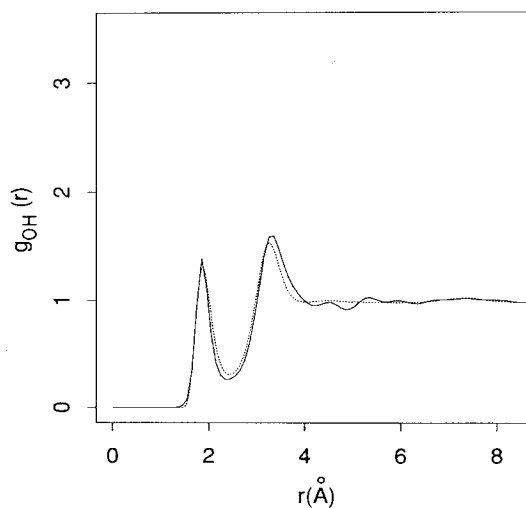


FIG. 11. Intermolecular pair cross-correlation function  $g_{OH}(r)$  for the  $\lambda=1$ , 25°C liquid (dotted curve). The Soper-Phillips experimental determination (Ref. [26]) is included for comparison (solid curve).

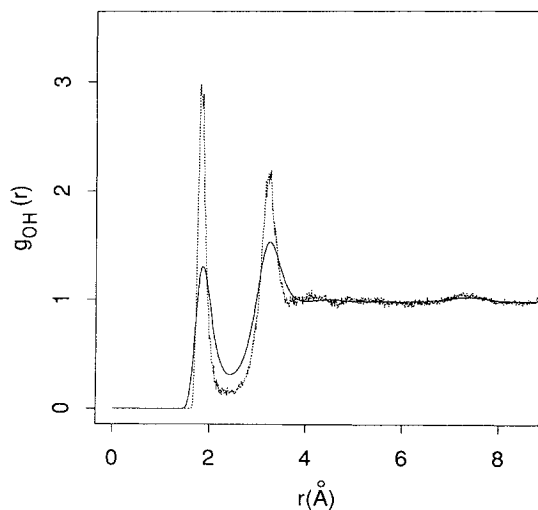


FIG. 12. Intermolecular pair cross-correlation function for the  $\lambda=1$  inherent structures (dotted curve), and for the unmapped simulation liquid at 25°C.

obviously occurred, though the distribution continues to be essentially flat at large separations. Notice that the minimum of  $g_{OH}(r)$  for inherent structures, between the first and second peaks, although lower than that before mapping, remains significantly above zero. Using the prior  $r_c(OH)$  again, the mean number of neighboring H's around an O has climbed to 1.96.

## V. CONCLUSIONS

Except for relatively minor discrepancies, the  $\lambda=0$  and  $\lambda=1$  liquids at 25°C appear to have the same oxygen-atom pair short-range order. No doubt, some small refinements in  $v_0$  and  $v_1$  (i.e.,  $V^{(2)}$ ) could cause the  $g_{OO}$ 's for these cases to agree perfectly with each other at 25°C, as well as with the experimentally determined function. It is important though to note that in spite of essential agreement at the oxygen pair correlation level, the statistical structures of the  $\lambda=0$  and 1 cases are *not* the same. In particular, the premapping neighbor angle distributions shown in Figs. 6 and 9 are quantitatively quite different. Furthermore, the first and third data columns in Table I reveal significant differences. These contrasts reflect distinct three-body, four-body, etc., correlations for the two cases, that are clearly undetermined by two-body correlations. This situation provides an undermining counterexample to the validity of the so-called "inverse Monte Carlo method," [30–33] an approach which attempts to reconstruct full statistical structure given only correlation information at the pair level.

The vivid differences between the  $g_{OO}$ 's for  $\lambda=0$  and 1 inherent structures, Figs. 5 and 8, show that the nearly identical 25°C distributions of oxygen pairs are produced in rather different ways. But, in both cases,  $\lambda=0$  and 1, the vibrational excitations out of the corresponding sets of inherent structures must be significantly anharmonic; this is demonstrated by the fact that the thermal energy increments shown in Eqs. (3.1) and (4.1) substantially

exceed the respective harmonic-oscillator equipartition values  $\frac{3}{2}k_B T$  and  $3k_B T$ .

Our water simulations are consistent with those of others that have examined inherent structures [15,17], in particular with respect to the importance of coordination numbers differing from 4 [16]. From the point of view of the statistical thermodynamic perturbation theory for water [28] it is pleasing to verify that coordination defects are even present in the unperturbed reference state defined by  $\Phi_0$ .

It has been pointed out before that coordination numbers greater than four are probably important for molecular mobility in liquid water [16], and in particular may be associated with bifurcated hydrogen bonds (an H shared by two acceptor O's in a pair of nonlinear H bonds) [34]. As liquid water is cooled down to its melting point, and especially down through the supercooling regime, apparently the mean coordination number approaches 4 more closely. Almost certainly the same is expected for the corresponding inherent structures. Strong supercooling entails substantial density decrease accompanied by substantial increase in overall binding energy [35]. This is compelling evidence that coordination defects are annealed out by the constant pressure supercooling, to produce near the supercooling limit (–46°C) a virtually perfect random tetrahedral hydrogen-bond network. The activation energy for the strongly non-Arrhenius shear viscosity confirms this view; it climbs from about 4.2 kcal/mol at room temperature to at least 14 kcal/mol at –35°C [36]. Bifurcated hydrogen bonds may well facilitate shear flow at room temperature, but are apparently largely unavailable at the low-temperature limit to mediate network restructuring. Only a more energy-costly tear and repair mechanism may be available [37].

As we have defined the liquid-water perturbation problem,  $\Phi_0$  in principle will be temperature and density dependent. Unfortunately, adequate experimental data for  $g_{OO}(r)$  over wide temperature and density ranges are not yet available. We look forward to a change in this situation, and to the opportunity to examine  $\lambda=0$  and 1 inherent structures in the strongly supercooled regime to assess the qualitative picture just outlined.

Even though our calculations have been limited to the 25°C equilibrium liquid state (and its inherent structures), an important concept has emerged. By contrast with the isotropically interacting  $\lambda=0$  system, the presence of directional hydrogen bonds at  $\lambda=1$  plays an important role in establishing and maintaining the many-molecule arrangements that dominate system properties. This is clear from the greater resistance of the  $\lambda=1$  system to vibrational delocalization in comparison with  $\lambda=0$ , whether pair-correlation functions are examined, or higher-order correlation measures.

## APPENDIX A

The central interaction  $v_0(r)$  was determined numerically from experimental input as described in Sec. II above. The tabular results subsequently were fitted with a finite combination of elementary functions. Specifically

we have used the form

$$v_0(r) = \varepsilon[(\sigma/r)^a - (\sigma/r)^b] + \sum_{i=1}^4 h_i \exp\{ -[(r - c_i)/w_i]^2 \}. \quad (\text{A1})$$

Using, respectively, Å and kcal/mol as the length and energy units, the 16 parameters have the following numerical values:

$$\begin{aligned} \varepsilon &= 6.014 \times 10^{-3}, \quad \sigma = 4.218, \\ a &= 9.056, \quad b = 4.044, \\ h_1 &= -1.132, \quad c_1 = 2.845, \quad w_1 = 0.257, \\ h_2 &= 1.664, \quad c_2 = 2.204, \quad w_2 = 1.945, \\ h_3 &= -0.672, \quad c_3 = 4.489, \quad w_3 = 2.183, \\ h_4 &= 0.266, \quad c_4 = 5.527, \quad w_4 = 0.577. \end{aligned} \quad (\text{A2})$$

#### APPENDIX B

The pair interaction operative between fully coupled water molecules has been denoted by  $V^{(2)} \equiv v_0 + v_1$  in the

text. The specific case used for the Monte Carlo simulation conforms functionally to that of the ST2 potential [20], so we have

$$v_0 + v_1 = v_{\text{LJ}}(r_{ij}) + S(r_{ij})v_{\text{el}}(\mathbf{x}_i, \mathbf{x}_j). \quad (\text{B1})$$

Here  $v_{\text{LJ}}$  is a Lennard-Jones 12-6 pair interaction,  $S$  is a cubic spline function that interpolates smoothly between 0 (at small  $r_{ij}$ ) and 1 (at large  $r_{ij}$ ). The orientation-dependent function  $v_{\text{el}}$  represents electrostatic interactions between point charges, four rigidly affixed to each water.

The functions  $v_{\text{LJ}}$  and  $S$  remain the same as for the ST2 potential [20]. To improve Monte Carlo agreement with the Soper-Phillips experiment [26], it seemed advisable to modify the placement and magnitude of the point charges somewhat. The angle between the two negative charges representing "lone-pair electrons" has been increased from  $\theta_l$  to 134.44°. The angle between the "proton" charges continues to be  $\theta_l$ . The distances respectively to "lone-pair" and "proton" charges remain at 0.8 and 1.0 Å. Charge magnitudes have been increased from 0.2357e (ST2) to 0.2457e ( $v_0 + v_1$ ).

- 
- [1] F. H. Stillinger and T. A. Weber, *Phys. Rev. A* **25**, 978 (1982).
- [2] F. H. Stillinger and T. A. Weber, *Phys. Rev. A* **28**, 2408 (1983).
- [3] F. H. Stillinger, in *Mathematical Frontiers in Computational Chemical Physics*, edited by Donald G. Truhlar, IMA Volumes in Mathematics and Its Applications Vol. 15 (Springer-Verlag, New York, 1988), pp. 157–173.
- [4] F. H. Stillinger and T. A. Weber, *J. Chem. Phys.* **80**, 4434 (1984).
- [5] F. H. Stillinger and T. A. Weber, *Phys. Rev. B* **31**, 5262 (1985); **33**, 1451(E) (1986).
- [6] T. A. Weber and F. H. Stillinger, *Phys. Rev. B* **32**, 5402 (1985).
- [7] F. H. Stillinger, *J. Chem. Phys.* **88**, 7818 (1988).
- [8] R. Elber and M. Karplus, *Science* **235**, 318 (1987).
- [9] R. Zwanzig, *J. Chem. Phys.* **79**, 4507 (1983).
- [10] J. Haffner, *J. Phys. F* **18**, 153 (1988).
- [11] D. Thirumalai, *J. Phys. Chem.* **93**, 5637 (1989).
- [12] W. C. Swope and H. C. Andersen, *Phys. Rev. B* **41**, 7042 (1990).
- [13] F. H. Stillinger and T. A. Weber, *J. Phys. Chem.* **87**, 2833 (1983).
- [14] T. A. Weber and F. H. Stillinger, *J. Chem. Phys.* **80**, 438 (1984).
- [15] A. Pohorille, L. R. Pratt, R. A. La Violette, M. A. Wilson, and R. D. MacElroy, *J. Chem. Phys.* **87**, 6070 (1987).
- [16] F. Sciortino, A. Geiger, and H. E. Stanley, *J. Chem. Phys.* **96**, 3857 (1992).
- [17] I. Ohmine, H. Tanaka, and P. Wolynes, *J. Chem. Phys.* **89**, 5852 (1988).
- [18] H. Tanaka and I. Ohmine, *J. Chem. Phys.* **91**, 6318 (1989).
- [19] I. Ohmine and H. Tanaka, *J. Chem. Phys.* **93**, 8138 (1990).
- [20] A. Rahman and F. H. Stillinger, *J. Am. Chem. Soc.* **95**, 7943 (1973).
- [21] O. Matsuoka, E. Clementi, and M. Yoshimine, *J. Chem. Phys.* **64**, 1351 (1976).
- [22] W. L. Jorgensen, J. Chandrasekhar, J. D. Madura, R. W. Impey, and M. L. Klein, *J. Chem. Phys.* **79**, 926 (1983).
- [23] H. J. C. Berendsen, J. P. M. Postma, W. F. van Gunsteren, and J. Hermans, in *Intermolecular Forces*, edited by B. Pullman (Riedel, Dordrecht, 1981), p. 331.
- [24] J. P. Hansen and I. R. McDonald, *Theory of Simple Liquids*, 2nd ed. (Academic, New York, 1986), p. 119.
- [25] J. P. Hansen and I. R. McDonald, *Theory of Simple Liquids* (Ref. [24]), p. 106.
- [26] A. K. Soper and M. G. Phillips, *Chem. Phys.* **107**, 47 (1986).
- [27] J. P. Valleu and S. G. Whittington, in *Statistical Mechanics, Part A: Equilibrium Techniques*, edited by B. J. Berne (Plenum, New York, 1977), pp. 137–168.
- [28] T. Head-Gordon and F. H. Stillinger (unpublished).
- [29] D. Eisenberg and W. Kauzmann, *The Structure and Properties of Water* (Oxford University, New York, 1969); relevant thermodynamic data appear in Chaps. 3 and 4.
- [30] M. D. Reichtin, A. L. Renninger, and B. J. Averbach, *J. Non-Cryst. Solids* **15**, 74 (1974).
- [31] N. de la Rosa-Fox, L. Esquivias, P. Villares, and R. Jimenez-Garay, *Phys. Rev. B* **33**, 4094 (1986).
- [32] O. A. Evdokimenko, A. S. Shteinberg, and V. P. Alekhin, *Metallofizika* **9**, 124 (1987).
- [33] V. V. Alenkov, D. K. Belashchenko, and G. D. Kuznetsov, *Rasplavy* **3**, (1989) [Melts **3**, 257 (1990)].
- [34] P. A. Gigere, *J. Chem. Phys.* **87**, 4835 (1987).
- [35] R. J. Speedy, *J. Phys. Chem.* **91**, 3354 (1987).
- [36] C. A. Angell, in *Water, A Comprehensive Treatise*, edited by F. Franks (Plenum, New York, 1982), Vol. 7, p. 48.
- [37] F. H. Stillinger, *J. Chem. Phys.* **89**, 6461 (1988).